Generalization of ETS-NOCV and ALMO-COVP Energy Decomposition Analysis to Connect Any Two Electronic States and Comparative Assessment

Hengyuan Shen,[†,‡] Zhenling Wang,[†,‡] and Martin Head-Gordon[*,†]

†*Pitzer Center for Theoretical Chemistry, Department of Chemistry, University of California, Berkeley, California 94720, USA*

‡*Contributed equally to this work*

E-mail: mhg@cchem.berkeley.edu

Abstract

Energy decomposition analysis (EDA) is a useful tool for obtaining chemically meaningful insights into molecular interactions. The extended transition state method with natural orbitals for chemical valence (ETS-NOCV) and the absolutely localized molecular orbital based method with complementary occupied-virtual pairs (ALMO-COVP) are two successful EDA schemes. Working within ground state generalized Kohn-Sham density functional theory (DFT), we extend these methods to do EDA between any two electronic states that can be connected by a unitary transformation of density matrices. A direct proof that the NOCV eigenvalues are symmetric pairs is given, and we also prove that the charge and energy difference defined by ALMO is invariant under certain orbital rotations, allowing us to define COVPs. We point out that ETS is actually a 1-point quadrature to obtain the effective Fock

matrix, and though it is reasonably accurate, it can be systematically further improved by adding more quadrature points. We explain why the calculated amount of transferred charge measured by ALMO-COVP is typically much smaller than that of ETS-NOCV, and explain why the ALMO-COVP values should be preferred. While the two schemes are independent, ETS-NOCV and ALMO-COVP in fact give a very similar chemical picture for a variety of chemical interactions, including H – H^+, the transition structure for the Diels-Alder reaction between ethene and butadiene, and two hydrogen-bonded complexes, $H_2O \cdots F^-$, and $H_2O \cdots HF$.

1 Introduction

Modern quantum chemistry methods are able to predict binding energies of most intermolecular interactions to a high level of accuracy;[1] however, binding energy alone does not reveal much detail about the physical origin of a given intermolecular interaction.[2] In order to obtain more chemical insights about intermolecular interactions, various energy decomposition analysis (EDA)[3–6] schemes were devised to further break the binding energies into physically intuitive terms, such as electrostatics, dispersion, polarization, and charge transfer. Unfortunately, due to the lack of associated observables, the resulting decompositions of energy cannot be uniquely defined in the overlapping region, though a well-designed EDA should be able to demonstrate the asymptotic behaviors of these terms in the long-range interaction limit. Links to observables are also possible by differentiating intermediate energies.[7,8]

Mean-field theories based on self-consistent field (SCF) calculations, such as Hartree-Fock (HF) and density functional theory (DFT), are among the most economical quantum chemistry methods. With the development of modern density functionals, DFT calculations are also capable of yielding accurate results for intermolecular interactions.[1] Accordingly, many useful EDA schemes have been developed based on mean-field theories. The seminal Kitaura-Morokuma EDA (KM-EDA)[9–11] decomposes the HF interaction energy into

electrostatic, Pauli repulsion, polarization and charge transfer contributions. The widely used extended transition state method combined with natural orbitals for chemical valence theory (ETS-NOCV)[12–14] decomposes the DFT interaction energy into electrostatics, Pauli repulsion, and orbital interaction terms.

An important improvement to the KM-EDA for HF and DFT calculation is the variational treatment of polarization, where the polarized state is obtained by minimizing energy of the super-system without breaking the fragment block-diagonal structure of the molecular orbital (MO) coefficient matrix through self-consistent field for molecular interaction (SCF-MI) calculations.[15,16] The resulting absolutely localized MOs (ALMOs)[17] are used in the block-localized wavefunction EDA (BLW-EDA)[18–20] and ALMO-EDA,[21–24] both of which break the interaction energy into frozen (FRZ), polarization (POL) and charge transfer (CT) terms. The frozen energy is the energy change from the isolated fragments with their MOs separately optimized to the frozen state which is obtained by a direct antisymmetrization of the fragment wavefunctions. The polarization energy is associated with the relaxation of each fragment's MOs in the presence of other fragments, and the charge transfer energy is the energy decrease due to interfragment orbital mixing. However, in the large basis limit, MOs on different fragments may have considerable overlap, and this will introduce CT contamination into the polarized state. The second generation of ALMO-EDA fixed this problem by keeping only the fragment electric response functions (FERFs)[25] in the virtual space during the SCF-MI calculation. Since the FERFs describe in the most compact way the orbital response to electric field components, a useful polarized state can be obtained even at the complete basis set limit.

The NOCV component[26 27 28] of the ETS-NOCV EDA diagonalizes the difference density matrix between the FRZ and CT states, which yields a set of orbital pairs that correspond to the electron density removed from the initial state and rearranged in the final state, with corresponding eigenvalues giving the numbers of electrons rearranged in each "transition". In favorable cases only one or two eigenvalues are significantly non-zero, and therefore an orbital

picture can be associated with the density changes associated with the ETS-NOCV EDA. This facilitates chemical interpretation. In a related way, the electron density rearrangement associated with CT in the ALMO-EDA can be given an orbital interpretation using the complementary occupied-virtual pairs (COVP) analysis.[29,30] COVP analysis singular value decomposes the generator of the unitary transformation associated with CT, leading to a set of singular values, and one occupied orbital for each singular value. In favorable cases, only one or two singular values are significant, which facilitates an easy-to-visualize orbital picture of the donor and acceptor orbitals that play the most important roles in charge transfer. Thus both NOCV-EDA and the COVP analysis in ALMO-EDA are successful in explaining CT effects on intermolecular interactions such as dative bonding[30] and transition metal complexes,[26] and even give us some insights about chemical reactions.[31] Yet to date, there has been no effort to develop connections between these two methods of analysis; that is our purpose in this work.

Specifically, we try to elaborate the connections between the orbital interaction energy of ETS-NOCV EDA and the polarization and charge transfer energy of ALMO-COVP EDA, which both describes the energy decrease obtained from relaxing the super-system from the directly antisymmetrized frozen state (FRZ) to the fully relaxed charge transfer state (CT). We will show that the orbital interaction energy of ETS-NOCV EDA can be decomposed into the same POL and CT terms as those in ALMO-COVP EDA by using the same intermediate polarized state. We note that this further decomposition of the orbital interaction of ETS-NOCV EDA has been done before by inserting the polarized state obtained from an SCFMI calculation.[32] However, inclusion of the whole virtual space during SCFMI results in a CT contaminated polarized state as the complete basis set limit is approached.[33–35] This can be resolved by keeping only the FERFs in the virtual space to achieve a polarized state with a useful basis set limit.[25] Another issue to be discussed is the question of how well that ETS-NOCV EDA and the COVP approach measure the amount of charge transferred – which is an important and sometimes controversial question.[35,36] ETS-NOCV EDA is well known

to overestimate the amount of transferred charge compared with other EDA schemes.[37] We will reveal the (significant) extent of the discrepancy in charge transfer obtained from these two EDA schemes by working out their exact mathematical expressions separately, and then provide an interpretation of this difference. The next part of our analysis establishes that the NOCV and COVP orbitals themselves are actually closely related: both are valid approaches that in fact provide very similar chemical interpretation as well as energy decomposition.

This paper is organized as follows. We first provide theories of a generalized ETS-NOCV method and ALMO-COVP method that can do energy decomposition between any two electronic states that can be represented as single determinants (i.e. generalized Kohn-Sham theory), and present the energy and charge decomposition expressions respectively. Then the simple example of H_2^+ is used to explain the charge transfer discrepancies obtained from these two EDA schemes. Finally, we present results for a Diels-Alder reaction and two hydrogen-bonding systems to illustrate the similar chemical interpretations provided by both EDA schemes.

2 Theory

2.1 Notation

We adopt the following notation in the subsequent derivations. Latin letters x, y, z are used to denote fragments, letters i, j, k are used to label occupied molecular orbitals, letters a, b, c are used to label virtual molecular orbitals, letters r, s, t are used to label general molecular orbitals, and Greek letters α, β, γ are used to label atomic orbitals. We denote molecular orbitals as $|\psi\rangle$ and atomic orbitals as $|\phi\rangle$. o and v refer to the total number of occupied and virtual MOs, respectively, while n refers to the total number of MOs. The AO overlap matrix is defined as $S_{\alpha\beta} = \langle\phi_\alpha|\phi_\beta\rangle$, the MO overlap matrix is defined as $\sigma_{rs} = \langle\psi_r|\psi_s\rangle$, and the occupied MO overlap matrix is defined as $(\sigma_o)_{xi,yj} = \langle\psi_{xi}|\psi_{yj}\rangle$. Since the ALMOs from one fragment are not guaranteed to be orthogonal to those from another fragment, we also

need the biorthogonal ALMO basis functions,[38] which are denoted with a superscript

$$|\psi^{xr}\rangle = \sum_{ys}^{n} (\sigma^{-1})_{ys,xr} |\psi_{ys}\rangle; \tag{1}$$

Similarly, the projector onto the occupied subspace can be written as

$$\hat{R} = \sum_{xi}^{o} |\psi_{xi}\rangle\langle\psi^{xi}| = \sum_{xi,yj}^{o} |\psi_{xi}\rangle(\sigma_o^{-1})_{yj,xi}\langle\psi_{yj}|. \tag{2}$$

The virtual space projector $\hat{Q}$ can be constructed from projected virtual orbitals $|\tilde{\psi}_{xa}\rangle = (\hat{1} - \hat{R})|\psi_{xa}\rangle$:

$$\hat{Q} = \hat{1} - \hat{R} = \sum_{xa}^{v} |\tilde{\psi}_{xa}\rangle\langle\tilde{\psi}^{xa}| = \sum_{xa,yb}^{v} |\tilde{\psi}_{xa}\rangle(\tilde{\sigma}_v^{-1})_{yb,xa}\langle\tilde{\psi}_{yb}| \tag{3}$$

with $(\tilde{\sigma}_v)_{xa,yb} = \langle\tilde{\psi}_{xa}|\tilde{\psi}_{yb}\rangle$. For simplicity, we use $|\psi_{xa}\rangle$ to denote the projected virtual orbitals $|\tilde{\psi}_{xa}\rangle$ from now on. We used real orbitals in this paper, but the generalization to complex orbitals can be similarly derived.

2.2 Construction of NOCVs and the associated ETS-NOCV EDA

The NOCV[14] orbitals, $|\varphi_i\rangle$, are defined as the eigenvectors of the difference of density operators between an initial state i and a final state f, which satisfies

$$\Delta\hat{P}|\varphi_i\rangle = (\hat{P}_f - \hat{P}_i)|\varphi_i\rangle = \lambda_i|\varphi_i\rangle \tag{4}$$

where $\hat{P}_i$ and $\hat{P}_f$ are the initial and final density operators, and λ_i is the corresponding eigenvalue. Since the two states have the same number of electrons, we immediately get $\mathrm{Tr}\left\{\Delta\hat{P}\right\} = 0$, and it turns out the eigenvalues of NOCVs always come out as symmetric pairs $\pm\lambda_i$ or 0.[39] Here we present a new proof of the above property by representing $\Delta\hat{P}$ in an orthonormal basis and directly working out the eigenvalue by performing Singular Value Decomposition (SVD) to simplify the matrix form, which will also reveal a deeper connection

between the ETS-NOCV EDA and the ALMO-COVP EDA.

We will work in an orthonormal eigen-basis of $\hat{P}_i$ so that the matrix representation of $\hat{P}_i$ is

$$P_i = \begin{pmatrix} I & 0 \\ 0 & 0 \end{pmatrix}, \tag{5}$$

where I is an identity matrix of dimension $o \times o$ and the diagonal 0 matrix is of dimension $v \times v$. P_f can be constructed from a unitary transformation of P_i as

$$P_f = \exp\{X\} P_i \exp\{-X\} \tag{6}$$

When P_i and P_f are derived from single determinants, X can be parameterized by the $o \times v$ rectangular generator matrix X_{ov}

$$X = \begin{pmatrix} 0 & X_{ov} \\ -X_{ov}^T & 0 \end{pmatrix}. \tag{7}$$

$\exp\{X\}$ is then explicitly given as[40,41]

$$\exp\{X\} = \begin{pmatrix} \cos Z^{1/2} & Z^{-1/2} \sin Z^{1/2} X_{ov} \\ -X_{ov}^T Z^{-1/2} \sin Z^{1/2} & \cos Y^{1/2} \end{pmatrix}, \tag{8}$$

where $Z = X_{ov} X_{ov}^T$ and $Y = X_{ov}^T X_{ov}$. Therefore, the explicit form of ΔP is

$$\Delta P = \begin{pmatrix} \cos Z^{1/2} \cos Z^{1/2} - I & -\cos Z^{1/2} Z^{-1/2} \sin Z^{1/2} X_{ov} \\ -X_{ov}^T Z^{-1/2} \sin Z^{1/2} \cos Z^{1/2} & X_{ov}^T Z^{-1/2} \sin Z^{1/2} Z^{-1/2} \sin Z^{1/2} X_{ov} \end{pmatrix}. \tag{9}$$

We will focus on the analysis for $o < v$, which is the most common case in real applications. Using the SVD of X_{ov}, we have $X_{ov} = U \Sigma V^T$, where U and V are two orthonormal matrices of dimensions $o \times o$ and $v \times v$, and Σ is a rectangular diagonal matrix of dimension

$o \times v$. This gives us $Z = U\Sigma\Sigma^T U^T = U\Sigma'^2 U^T$, where $\Sigma' = \mathrm{diag}(\sigma_1, \sigma_2, ..., \sigma_o)$. As a result, $Z^{1/2} = U\Sigma' U^T$. With the help of these matrices, we can further simplify ΔP as

$$\Delta P = \begin{pmatrix} U & 0 \\ 0 & V \end{pmatrix} \begin{pmatrix} -\sin^2\Sigma' & -\cos\Sigma'\Sigma'^{-1}\sin\Sigma'\Sigma \\ -\Sigma^T\Sigma'^{-1}\sin\Sigma'\cos\Sigma' & \Sigma^T\Sigma'^{-1}\sin\Sigma'\Sigma'^{-1}\sin\Sigma'\Sigma \end{pmatrix} \begin{pmatrix} U^T & 0 \\ 0 & V^T \end{pmatrix}, \quad (10)$$

and since $\Sigma = (\Sigma', 0)$, where 0 is of dimension $o \times (v - o)$,

$$\Delta P = \begin{pmatrix} U & 0 \\ 0 & V \end{pmatrix} \begin{pmatrix} -\sin^2\Sigma' & -\cos\Sigma'\sin\Sigma' & 0 \\ -\sin\Sigma'\cos\Sigma' & \sin^2\Sigma' & 0 \\ 0 & 0 & 0 \end{pmatrix} \begin{pmatrix} U^T & 0 \\ 0 & V^T \end{pmatrix}. \quad (11)$$

It is now clear that we get at least $v - o$ NOCVs with eigenvalue 0, while the non-zero eigenvalues can be obtained by diagonalizing the inner matrix, which is equivalent to diagonalizing a set of 2 by 2 matrices of the structure

$$\begin{pmatrix} -\sin^2\sigma_i & -\cos\sigma_i\sin\sigma_i \\ -\sin\sigma_i\cos\sigma_i & \sin^2\sigma_i \end{pmatrix}. \quad (12)$$

Notice that if $\sin\sigma_i = 0$, the diagonalization of this sub-matrix still gives us NOCVs with eigenvalue 0, so we assume $\sin\sigma_i \neq 0$ to get nontrivial NOCVs. Solving a simple quadratic equation in terms of the eigenvalue λ_i gives us $\lambda_i = \pm\sin\sigma_i$, and it is clear that there are at most o such pairs.

For the other case where $o \geq v$, we can do the thin SVD of X_{ov}, so that $X_{ov} = U\Sigma' V^T$, where U is a matrix of dimension $o \times v$ with orthonormal columns, V is an orthonormal matrix of dimension $v \times v$, and $\Sigma^{'}$ is a diagonal $v \times v$ matrix. Then, all the further derivations are the same except no 0 blocks appear as in the inner matrix of Eqn.(11), and therefore we get at most v pairs of NOCVs.

In summary, for a system state with o occupied orbitals and v virtual orbitals, there will

be at most $\min(o, v)$ pairs of NOCVs with non-zero eigenvalue $\pm \sin \sigma_i$, where σ_i are the singular values of the generator X_{ov}. Since we assumed nothing more than an orthonormal basis of P_i, this conclusion should hold for any SCF calculation, as long as P_f is obtainable from a unitary transformation of P_i.

As a result, we can decompose the difference between two density operators as

$$\Delta \hat{P} = \sum_{i}^{o} \lambda_i \left(|\varphi_i\rangle\langle\varphi_i| - |\varphi_{-i}\rangle\langle\varphi_{-i}| \right), \tag{13}$$

where $|\varphi_i\rangle$ and $|\varphi_{-i}\rangle$ are NOCVs with paired positive and negative eigenvalues, and in the summation we only sum over the positive eigenvalues. Thus, the density change associated with each NOCV pair is $\Delta\rho(\vec{r})_i = \lambda_i \left(|\varphi_i(\vec{r})|^2 - |\varphi_{-i}(\vec{r})|^2 \right)$, which can provide a visualization of the density rearrangement. Since we already have the eigenvalues of ΔP, Eqn.(11) gives us

$$|\varphi_{\pm i}\rangle = \begin{pmatrix} U & 0 \\ 0 & V \end{pmatrix} |v_{\pm i}\rangle, \tag{14}$$

where $|v_{\pm i}\rangle$ is represented by vector $(0, ..., 1, ..., 0, 0, ..., (-\sin \sigma_i \mp 1)/\cos \sigma_i, ..., 0)$, with the only two non-zero elements at the ith and $(o+i)$th position. We can then directly calculate the occupation number of each NOCV in the initial and final state as

$$n_{\pm i}^{(i)} = \frac{\langle \varphi_{\pm i} | \hat{P}_i | \varphi_{\pm i} \rangle}{\langle \varphi_{\pm i} | \varphi_{\pm i} \rangle} = \frac{1}{2}(1 \mp \lambda_i), \tag{15}$$

$$n_{\pm i}^{(f)} = \frac{\langle \varphi_{\pm i} | \hat{P}_f | \varphi_{\pm i} \rangle}{\langle \varphi_{\pm i} | \varphi_{\pm i} \rangle} = \frac{1}{2}(1 \pm \lambda_i). \tag{16}$$

The interpretation of the occupation numbers is that from the initial state to the final state, λ_i electrons are transferred from the anti-bonding $|\varphi_{-i}\rangle$ to the bonding $|\varphi_i\rangle$, as was pointed out in reference.[26] Therefore, the total amount of charge transfer can be defined as

$$\Delta Q = \sum_{i}^{o} \lambda_i = \sum_{i}^{o} \sin \sigma_i. \tag{17}$$

In order to decompose the energy, we parametrize energy as $E(P(\lambda)) = E(P_i + \lambda\Delta P)$. Clearly, $E(\lambda = 0) = E_i$, $E(\lambda = 1) = E_f$. So

$$\begin{aligned}
\Delta E &= \int_0^1 \frac{\partial E}{\partial \lambda} \mathrm{d}\lambda \\
&= \int_0^1 \sum_{\alpha\beta}^{n} \frac{\partial E}{\partial P_{\alpha\beta}} \frac{\partial P_{\alpha\beta}}{\partial \lambda} \mathrm{d}\lambda \\
&= \sum_{\alpha\beta}^{n} \left(\int_0^1 F(\lambda)_{\alpha\beta} \mathrm{d}\lambda \right) \Delta P_{\alpha\beta} \\
&= \mathrm{Tr}\Big\{ F^{\mathrm{eff}} \Delta P \Big\} \\
&= \mathrm{Tr}\Big\{ \hat{F}^{\mathrm{eff}} \Delta \hat{P} \Big\},
\end{aligned} \tag{18}$$

where $\hat{F}^{\mathrm{eff}}$ is an effective fock operator. By insertion of the decomposition of $\Delta\hat{P}$, we get

$$\Delta E = \sum_{i}^{o} \lambda_i \left(\langle \varphi_i | \hat{F}^{\mathrm{eff}} | \varphi_i \rangle - \langle \varphi_{-i} | \hat{F}^{\mathrm{eff}} | \varphi_{-i} \rangle \right) = \sum_{i}^{o} \Delta E_i, \tag{19}$$

where

$$\Delta E_i = \lambda_i \left(\langle \varphi_i | \hat{F}^{\mathrm{eff}} | \varphi_i \rangle - \langle \varphi_{-i} | \hat{F}^{\mathrm{eff}} | \varphi_{-i} \rangle \right) = \lambda_i \sum_{\alpha\beta}^{n} \left(C_{i\alpha}^T F_{\alpha\beta}^{\mathrm{eff}} C_{\beta i} - C_{-i,\alpha}^T F_{\alpha\beta}^{\mathrm{eff}} C_{\beta,-i} \right) \tag{20}$$

is the energy associated with the ith NOCV pair, where C is the MO coefficient matrix of the NOCVs and $F_{\alpha\beta}^{\mathrm{eff}}$ is the matrix representation of $\hat{F}^{\mathrm{eff}}$ in the AO basis. The crucial step of the NOCV EDA is then to evaluate the effective fock matrix accurately. In a naive way, we can use one quadrature point to approximate the integral of Eq.(18), which gives us $F^{\mathrm{eff}} = F(\lambda = \frac{1}{2}) \times 1 = F(\frac{1}{2}P_i + \frac{1}{2}P_f) \approx \frac{1}{2}(F(P_i) + F(P_f))$. This formula is exact for Hartree-Fock calculation, whose fock matrix is a linear function of density matrix and is also called the "transition state" fock matrix used in the ETS-NOCV analysis.[14] Though our calculations on some example systems show that this 1-quadrature approximation is usually accurate up to 0.1 kJ/mol, the NOCV energy decomposition can be systematically

improved by approximating the integral with more quadrature points if this 1-quadrature approximation fails.

2.3 Construction of COVPs and the Associated EDA

In ALMO based EDA with COVP analysis, we define the total amount of charge transferred from the initial state to the final state as

$$\Delta Q = \mathrm{Tr}\Big\{\hat{R}_i\Big\} - \mathrm{Tr}\Big\{\hat{R}_i\hat{R}_f\Big\} = \mathrm{Tr}\Big\{\hat{R}_i\hat{Q}_f\Big\} = \mathrm{Tr}\Big\{\hat{R}_f\hat{Q}_i\Big\}, \tag{21}$$

which can be shown[30] to be the same as $2\,\mathrm{Tr}\Big\{\hat{R}^{\mathrm{eff}}_{vo}\hat{X}_{ov}\Big\}$, where $\hat{X}_{ov}$ is the generator of the unitary transformation that connects the initial and final density operators, and $\hat{R}^{\mathrm{eff}}_{vo}$ is an effective density operator with matrix elements $(R^{\mathrm{eff}}_{vo})_{ai} = -\int_0^1 R(\lambda X)_{ai}\; d\lambda$ in the orthonormal MO basis. By insertion of the projector into occupied and virtual space, we can break down the transferred charge into pairwise additive terms

$$\Delta Q = 2\,\mathrm{Tr}\Big\{\hat{R}\hat{R}^{\mathrm{eff}}_{vo}\hat{Q}\hat{X}_{ov}\Big\} = \sum_{xy}^{N_{\mathrm{frgm}}}\sum_{i}^{o_x}\sum_{a}^{v_y} 2\,\mathrm{Tr}\Big\{|\psi_{ya}\rangle\langle\psi^{ya}|\hat{R}^{\mathrm{eff}}_{vo}|\psi_{xi}\rangle\langle\psi^{xi}|\hat{X}_{ov}\Big\} = \sum_{xy}\Delta Q_{x\to y} \tag{22}$$

with $\Delta Q_{x\to y} = 2\sum_{ia}\langle\psi^{ya}|\hat{R}^{\mathrm{eff}}_{vo}|\psi_{xi}\rangle\langle\psi^{xi}|\hat{X}_{ov}|\psi_{ya}\rangle$ the amount of charge transferred from fragment x to fragment y.

We can work out ΔQ explicitly using the same matrix representations as we used in the last subsection, which gives

$$\Delta Q = \mathrm{Tr}\big\{I - \cos Z^{1/2}\cos Z^{1/2}\big\} = \mathrm{Tr}\big\{U\,(I - \cos\Sigma'\cos\Sigma')\,U^T\big\} = \sum_{i}^{o}\sin^2\sigma_i, \tag{23}$$

where σ_i are the singular values of X_{ov}. It is apparent that the amount of charge transfer defined in the COVP analysis will be generally smaller than that obtained in the NOCV analysis by directly comparing the explicit forms, this result is due to different definitions of charge transfer in the two EDA schemes, and the interpretation of this discrepancy will be

discussed in details later.

The energy in non-perturbative ALMO-COVP EDA is parameterized as $E(X^{'}(\lambda))$, with $X^{'} = \lambda X$ and X is that defined in Eq.(5). In this parameterization, $E(\lambda = 0) = E_i$, $E(\lambda = 1) = E_f$. So

$$\begin{aligned}
\Delta E &= \int_0^1 \frac{\partial E}{\partial \lambda} d\lambda \\
&= \int_0^1 \sum_{ia} \left(\frac{\partial E}{\partial X'_{ia}} X_{ia} \right) d\lambda \\
&= 2\,\mathrm{Tr}\big\{ F^{\mathrm{eff}}_{vo} X_{ov} \big\} \\
&= 2\,\mathrm{Tr}\Big\{ \hat{F}^{\mathrm{eff}}_{vo} \hat{X}_{ov} \Big\},
\end{aligned} \tag{24}$$

where

$$(F^{\mathrm{eff}}_{vo})_{ai} = \frac{1}{2} \int_0^1 \frac{\partial E}{\partial X'_{ia}} d\lambda \tag{25}$$

and the explicit form for the evaluation of F^{eff}_{vo} can be found in previous works.[30] Using a similar manipulation as we did to the transferred charge, we can break ΔE into pairwise additive terms, and the energy transfer from fragment x to fragment y is

$$\Delta E_{x\to y} = 2 \sum_{ia} \langle \psi^{ya} | \hat{F}^{\mathrm{eff}}_{vo} | \psi_{xi} \rangle \langle \psi^{xi} | \hat{X}_{ov} | \psi_{ya} \rangle. \tag{26}$$

In order to get the COVPs, we need a property that $\Delta Q_{x\to y}$ and $\Delta E_{x\to y}$ is unchanged under rotation of the occupied orbitals in fragment x and virtual orbitals in fragment y, which was stated before[29] but lacks a rigorous proof. This can be proved by directly evaluating the overlap matrix of rotated orbitals, and we will only show the proof for the occupied orbitals, since the proof for the virtual orbitals are similar. Consider an unitary matrix that rotates

the occupied orbitals $\{|\psi_{xi}\rangle\}$ of fragment x into $\{|\psi'_{xi}\rangle\}$

$$|\psi'_{xi}\rangle = \sum_{xj}^{o_x} U^{(x)}_{xj,xi}|\psi_{xj}\rangle, \tag{27}$$

$$|\psi'_{zi}\rangle = |\psi_{zi}\rangle, \tag{28}$$

where $\{|\psi_{zi}\rangle\}$, which denotes the occupied orbitals of other fragments, are left unchanged. Therefore, the overlap matrix of the rotated occupied orbitals is

$$\sigma'_o = \begin{pmatrix} U^{(x)T}(\sigma_o)_{xx}U^{(x)} & U^{(x)T}(\sigma_o)_{xz} \\ (\sigma_o)_{zx}U^{(x)} & (\sigma_o)_{zz} \end{pmatrix} = \begin{pmatrix} U^{(x)T} & 0 \\ 0 & I \end{pmatrix} \begin{pmatrix} (\sigma_o)_{xx} & (\sigma_o)_{xz} \\ (\sigma_o)_{zx} & (\sigma_o)_{zz} \end{pmatrix} \begin{pmatrix} U^{(x)} & 0 \\ 0 & I \end{pmatrix}, \tag{29}$$

and it is apparent that its inverse matrix is

$$(\sigma'_o)^{-1} = \begin{pmatrix} U^{(x)T} & 0 \\ 0 & I \end{pmatrix} \begin{pmatrix} (\sigma_o^{-1})_{xx} & (\sigma_o^{-1})_{xz} \\ (\sigma_o^{-1})_{zx} & (\sigma_o^{-1})_{zz} \end{pmatrix} \begin{pmatrix} U^{(x)} & 0 \\ 0 & I \end{pmatrix} = \begin{pmatrix} U^{(x)T}(\sigma_o^{-1})_{xx}U^{(x)} & U^{(x)T}(\sigma_o^{-1})_{xz} \\ (\sigma_o^{-1})_{zx}U^{(x)} & (\sigma_o^{-1})_{zz} \end{pmatrix}. \tag{30}$$

Therefore, the biorthogonal MOs of occupied orbitals located in fragment x is

$$|\psi'^{xi}\rangle = \sum_{zj}^{o} (\sigma')^{-1}_{zj,xi}|\psi'_{zj}\rangle = \sum_{xj}^{o_x} \left[U^T(\sigma_o^{-1})_{xx}U\right]_{xj,xi} |\psi'_{xj}\rangle + \sum_{zj\notin x}^{o} \left[(\sigma_o^{-1})_{zx}U\right]_{zj,xi} |\psi'_{zj}\rangle \tag{31}$$

$$= \sum_{xj,xk}^{o_x} \left[U^T(\sigma_o^{-1})_{xx}U\right]_{xj,xi} U_{xk,xj}|\psi_{xk}\rangle + \sum_{zj\notin x}^{o} \left[(\sigma_o^{-1})_{zx}U\right]_{zj,xi} |\psi_{zj}\rangle \tag{32}$$

$$= \sum_{xk}^{o_x} \left[(\sigma_o^{-1})_{xx}U\right]_{xk,xi} |\psi_{xk}\rangle + \sum_{zj\notin x}^{o} \left[(\sigma_o^{-1})_{zx}U\right]_{zj,xi} |\psi_{zj}\rangle \tag{33}$$

$$= \sum_{xj}^{o_x} U_{xj,xi}|\psi^{xj}\rangle, \tag{34}$$

and then it is obvious that $\sum_{xi}^{o_x} |\psi'_{xi}\rangle\langle\psi'^{xi}| = \sum_{xi}^{o_x} |\psi_{xi}\rangle\langle\psi^{xi}|$, and a similar derivation gives $\sum_{ya}^{v_y} |\psi'_{ya}\rangle\langle\psi'^{ya}| = \sum_{ya}^{v_y} |\psi_{ya}\rangle\langle\psi^{ya}|$ for virtual orbitals of fragment y. As a result,

$$\Delta E_{x\to y} = 2\sum_{ia}\langle\psi'^{ya}|\hat{F}^{\text{eff}}_{vo}|\psi'_{xi}\rangle\langle\psi'^{xi}|\hat{X}_{ov}|\psi'_{ya}\rangle, \tag{35}$$

$$\Delta Q_{x\to y} = 2\sum_{ia}\langle\psi'^{ya}|\hat{R}^{\text{eff}}_{vo}|\psi'_{xi}\rangle\langle\psi'^{xi}|\hat{X}_{ov}|\psi'_{ya}\rangle. \tag{36}$$

If we transform the occupied space and virtual space using the left and right orthonormal matrices in the singular value decomposition of $\langle\psi^{xi}|\hat{X}_{ov}|\psi_{ya}\rangle$, $\hat{X}_{ov}$ will be represented by a rectangular diagonal matrix with only $\min\{o_x, v_y\}$ non-zero entries under the basis $\{|\psi'^{xi}\rangle\}$ and $\{|\psi'_{ya}\rangle\}$. The $\min\{o_x, v_y\}$ pairs of the corresponding occupied and virtual orbitals $\{|\psi'_{xi}\rangle\}$ and $\{|\psi'_{ya}\rangle\}$ obtained in this way are called the complementary occupied-virtual pairs (COVPs), and they give the most compact description of the energy and charge transfer between the two fragments x and y. COVPs for other fragment pairs can be evaluated using similar method.

3 Computational Details

We separate the relaxation process from the directly antisymmetrized frozen state (FRZ) to the fully relaxed charge transfer state (CT) into two partial relaxations: (i) the polarization (POL) step and (ii) the charge transfer (CT) process. This is accomplished by inserting a polarization state (POL) into the path, which is obtained by performing self-consistent field for molecular interactions (SCF-MI)[15–17,22] calculations. The POL step is a constrained relaxation of each fragment in the presence of other fragments by mixing its occupied orbitals with only its own virtual orbitals.

The advantage of introducing this POL state is to better understand the response of the electron density of each fragment when the fragment is introduced into the environment of other fragments,[25] separate from permitting CT between fragments. This response

should contain at least electrical polarization and associated relaxation of Pauli repulsions. Introducing the POL state thus avoids "fragment self electron donation" during the charge transfer process. One could also introduce additional intermediate states (for instance separating components of CT such as forward and back donation[8]) since the theory presented above does not prevent us from doing so, although any such intermediate states should be physically meaningful to help us understand the interaction process.

In this article, we will study the POL and CT processes; for each process, both the ALMO-COVP EDA and ETS-NOCV EDA were performed. Only dipole and quadruple FERFs (DQ-FERFs)[23,25] were included in the virtual space of the SCF-MI calculation to get a well-defined POL state. By contrast, the total virtual space was used in the SCF calculation to get the fully relaxed CT state.

The calculations were performed in a development version of Q-Chem 5.4.[42] The ωB97X-D functional[43] with the def2-TZVPD basis set[44,45] were used for geometry optimization and vibrational mode analysis. The ωB97X-D functional with the aug-cc-pVTZ basis set[46–48] were used for the energy decomposition analysis unless otherwise specified. Geometries of $H_2O - F^-$ and $HF - H_2O$ complexes were confirmed to be local minima on the potential energy surface by showing that the Hessian matrix has no negative eigenvalues, and the geometry of the butadiene-ethene complex was confirmed to be a transition structure by showing that the Hessian matrix has exactly one negative eigenvalue.

Unless otherwise specified, all the COVPs and NOCVs were plotted with an isosurface value of ± 0.07 a.u. (blue for the positive isosurface and red for the negative isosurface). All the NOCV density difference plots were plotted with an isosurface value of ± 0.0005 a.u. (blue for the positive isosurface and red for the negative isosurface), and all the molecular figures were plotted using IQmol, the graphical user interface for Q-Chem. The occupied and virtual COVPs were plotted in solid and wire-frame style respectively. The NOCVs with positive and negative eigenvalues were plotted in solid and wire-frame style respectively, and the NOCV density differences were plotted in wire-frame style. All plots were generated

using Matplotlib.[49]

4 Results and Discussion

4.1 H_2^+ Molecular Ion

We first consider the simple H_2^+ cation to better understand the similarities and differences between the ALMO based COVP EDA and the ETS-NOCV EDA. The calculations were performed at the Hartree-Fock level of theory, which is exact for this one-electron problem, and the two fragments considered are a proton and a single hydrogen atom. Based on this choice, we expect important energetic contributions from both polarization and charge transfer at short range to form the 1-electron chemical bond, while at long range, both contributions eventually decay to zero.

Fig. 1 shows the energy decrease in the polarization and the charge transfer process obtained from ALMO-COVP EDA, ETS-NOCV EDA, and direct subtraction between final and initial state energies as we increase the distance r between the proton and hydrogen atom. For each point, the energy decrease calculated using these three methods agree with each other with errors less than 10^{-5} kJ/mol, which demonstrates the equivalence of these two EDA schemes. This high precision was achieved since we used 5 quadrature points to approximate the ALMO-COVP EDA effective Fock matrix shown in Eq. 25, while the ETS-NOCV EDA is exact for the Hartree-Fock method as pointed out before. In addition, the POL and CT energy decreases both demonstrate the correct asymptotic behavior of approaching zero as the distance, r between H and H^+ increases.

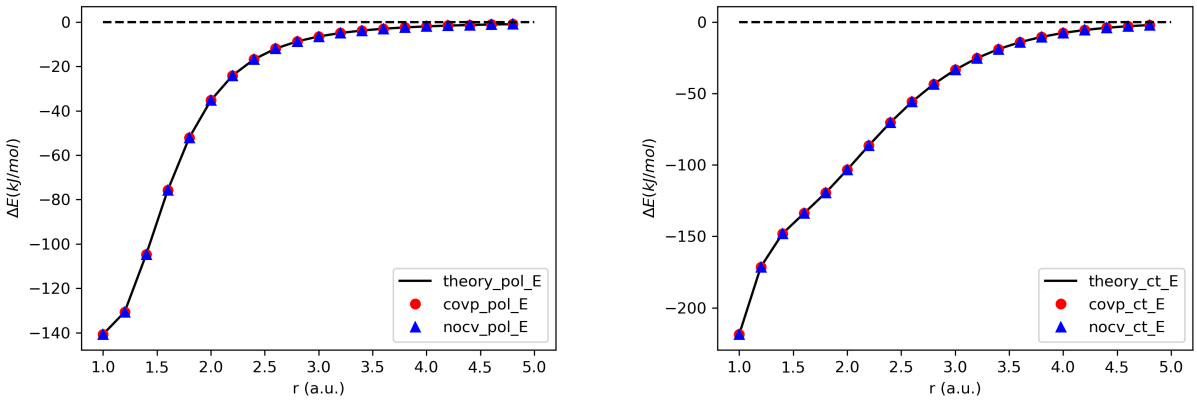

(a) POL ΔE (b) CT ΔE

Figure 1: (a) Energy decrease in the polarization process obtained from ALMO-COVP EDA (red line) with Eq. 24, ETS-NOCV EDA (blue line) with Eq. 18, and direct energy subtraction between the POL state and FRZ state as a function of distance between H and H^+. (b) Energy decrease in the charge transfer process obtained from ALMO-COVP EDA (red line), ETS-NOCV EDA (blue line), and direct energy subtraction between the CT state and POL state as a function of distance between H and H^+.

The amount of transferred charge obtained from these two EDA schemes apparently do not agree with each other, and the transferred charge calculated in ALMO-COVP EDA is much less than that obtained from ETS-NOCV EDA. From the exact expressions for the amount of transferred charge in Eqs. 17 and 23 and taking into account the fact that only one occupied orbital exists in H_2^+, we immediately reach the conclusion that the amount of transferred charge calculated using ETS-NOCV EDA is exactly the square root of that obtained from ALMO-COVP EDA. This is directly confirmed from the plots shown in Fig.2.

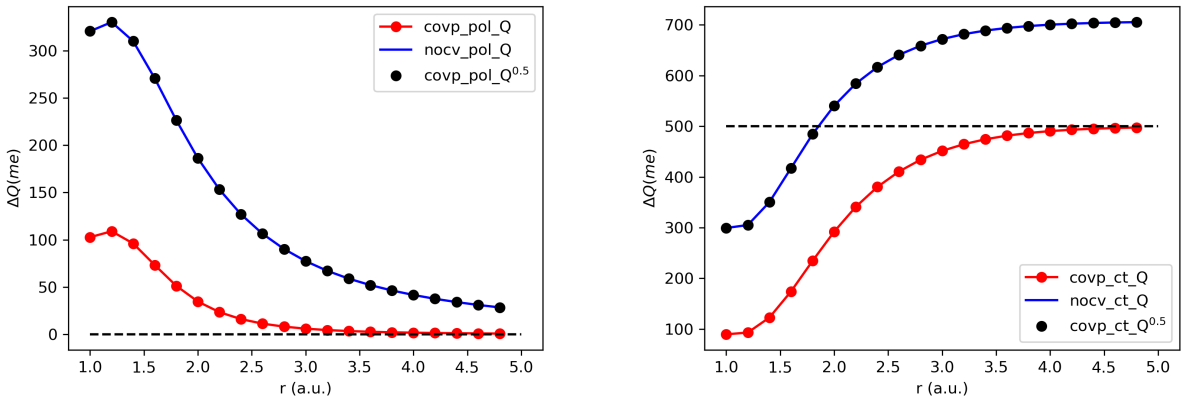

(a) POL ΔQ (b) CT ΔQ

Figure 2: (a) Amount of transferred charge in the polarization process obtained from ALMO-COVP EDA (red line) and ETS-NOCV EDA (blue line) as a function of distance between H and H^+. (b) Amount of transferred charge in the charge transfer process obtained from ALMO-COVP EDA (red line) and ETS-NOCV EDA (blue line) as a function of distance between H and H^+.

To better understand the discrepancies of transferred charge of these two EDA schemes, we take a further look at $r = 4.5$ a.u., where the proton and hydrogen atom are far enough from each other so that the polarization process is localized at the hydrogen atom, but the two particles are still weakly bound. The energy decrease in the polarization process is -1.18 kJ/mol, while it is -3.37 kJ/mol in the charge transfer process. The amount of transferred charge is 1.06 me^- for the polarization process and 495.89 me^- for the charge transfer process as calculated from ALMO-COVP EDA, while for ETS-NOCV EDA, it is 32.53 me^- for the polarization process and 704.19 me^- for the charge transfer process. In either EDA method, the amount of transferred charge during the polarization process is much less than that of the charge transfer process, as a result, we may approximate the amount of transferred charge in the charge transfer process as the amount of transferred charge from the FRZ state to the CT state. In the FRZ state, 1 electron is located at the hydrogen atom and 0 electron is found at the proton, while in the fully relaxed CT state, 1 electron is symmetrically distributed in the $H - H$ σ bond, resulting in a net amount of 0.5 electron at each hydrogen nucleus. This simple chemistry picture tells us that one would expect 0.5 electron being transferred from

the hydrogen to the proton, and the amount of transferred charge calculated using ALMO-COVP EDA agrees very well with this expectation, while ETS-NOCV evidently exaggerates the amount of transferred charge. This example suggests that the ALMO-COVP CTA is generally to be preferred over ETS-NOCV for estimates of the amount of transferred charge.

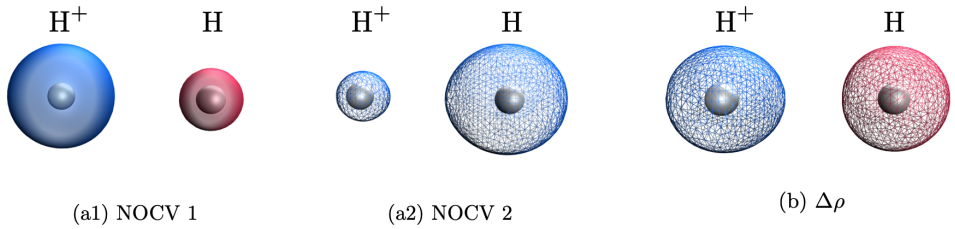

(a1) NOCV 1 (a2) NOCV 2 (b) $\Delta\rho$

Figure 3: (a)NOCVs of H_2^+ in the charge transfer process with (a1) positive and (a2) negative eigenvalues. (b)NOCV density difference plot (with isosurface value of ± 0.005) of H_2^+ in the charge transfer process.

An inspection of Fig.3 may help us understand why the ETS-NOCV EDA greatly overestimates the amount of transferred charge. Since the NOCVs are obtained by simply diagonalizing the difference of density matrices of POL and CT states, they can be delocalized over the whole system, which is confirmed by Fig. 3(a). However, the amount of transferred charge in ETS-NOCV EDA is defined as the number of electron moving from the NOCV with negative eigenvalue to the NOCV with positive eigenvalue. Because of delocalization, it is clear from Fig. 3(a) that this includes both electron moving from the hydrogen atom to the proton *and* electron moving from the hydrogen atom to itself. The latter flow of electron should not be counted towards the amount of charge transferred. However, the difference density shown in Fig. 3(b) nicely exhibits the net flow of electrons from the hydrogen atom to the proton. This demonstrates that *density difference plots of paired NOCVs* are a useful qualitative tool to understand the net direction of electron flow associated with a specific NOCV pair.

By contrast, in ALMO-COVP EDA, we treat the electrons in the common space of density matrices of initial and final states as unmoved, and the amount of transferred charge is defined

by the net flow of electrons, which is just the difference between the total number of electrons and the number of "immobile" electrons. For the FRZ state, we have $|\psi_{\mathrm{FRZ}}\rangle = |1s_{\mathrm{H}}\rangle$, and for the CT state, we roughly have $\sqrt{2}|\psi_{\mathrm{CT}}\rangle = |1s_{\mathrm{H}}\rangle + |1s_{\mathrm{H}^+}\rangle$. Taking into account the fact that $\langle 1s_{\mathrm{H}^+}|1s_{\mathrm{H}}\rangle \sim 0$ in the large $r_{\mathrm{H}-\mathrm{H}^+}$ limit and doing a simple calculation using our definition of the amount of transferred charge, we get $\Delta Q = 0.5\ e^-$, which agrees with the result of the intuitive argument.

4.2 Transition Structure for Cycloaddition of 1,3-Butadiene and Ethene

The interaction of 1,3-butadiene and ethene at their transition structure on the Diels-Alder cycloaddition pathway to cyclohexene serves as a good example with large energy decrease in the charge transfer process. The transition structure was calculated using the freezing string method[50] with the B3LYP[51,52] functional and the 6-31G* basis,[53,54] and the resulting geometry was confirmed to be a transition structure. We then performed EDA calculations at the B3LYP/aug-cc-pVTZ level of theory, where the two fragments were both treated as spin singlet state, following the reactants' perspective approach.[31] The main EDA results are summarized below in Table 1. It is apparent from Table 1 that both non-perturbative EDA methods give decomposed energies that agree very precisely with the total energy differences, confirming adequate quadrature accuracy with 5 points (COVP) and only 1 point (NOCV).

Table 1: Energies (in kJ/mol) and amounts of transferred charge (in me^-) calculated using ALMO-COVP EDA and ETS-NOCV EDA for the POL and CT processes.

	$E_{\mathrm{POL}} - E_{\mathrm{FRZ}}$	ΔE_{POL}	ΔQ_{POL}	$E_{\mathrm{CT}} - E_{\mathrm{POL}}$	ΔE_{CT}	ΔQ_{CT}
ALMO-COVP EDA	-30.97	-30.97	28.44	-173.75	-173.75	268.90
ETS-NOCV EDA	-30.97	-30.97	609.16	-173.75	-173.77	1339.18

Table 2: Significant COVPs of the POL and CT processes, as well as their associated energy decrease (in kJ/mol) and amounts of transferred charge (in me^-), and the percentage they contribute to the total energy decrease and amount of transferred charge for each process.

Pair	Donor	Acceptor	ΔE	$\Delta E/\Delta E_{\mathrm{POL}}(\%)$	ΔQ	$\Delta Q/\Delta Q_{\mathrm{POL}}(\%)$
1	C_4H_6	C_4H_6	-12.31	39.74	10.74	37.76
2	C_2H_4	C_2H_4	-7.73	24.96	7.09	24.94
3	C_4H_6	C_4H_6	-5.81	18.75	8.41	29.59

(a) Significant COVPs of POL process

Pair	Donor	Acceptor	ΔE	$\Delta E/\Delta E_{\mathrm{CT}}(\%)$	ΔQ	$\Delta Q/\Delta Q_{\mathrm{CT}}(\%)$
4	C_2H_4	C_4H_6	-84.71	48.75	154.75	57.55
5	C_4H_6	C_2H_4	-79.64	45.84	142.12	52.85

(b) Significant COVPs of CT process

By contrast, the amounts of transferred charge calculated with ETS-NOCV EDA are (excessively) larger than those obtained from ALMO-COVP EDA for each process, as expected from theory and the explanation provided for the H_2^+ example. An interesting observation is that for the POL process, the discrepancy between the amount of transferred charge obtained from these two EDA schemes is more severe than the case of CT process. This is because the CT process is compactly described by two COVPs only, while the POL process takes at least three COVPs to cover the total energy decrease. From Eqs. 17 and 23, the more significant COVPs we have, the greater the exaggeration in the amount of transferred charge we get using ETS-NOCV EDA versus ALMO-COVP EDA.

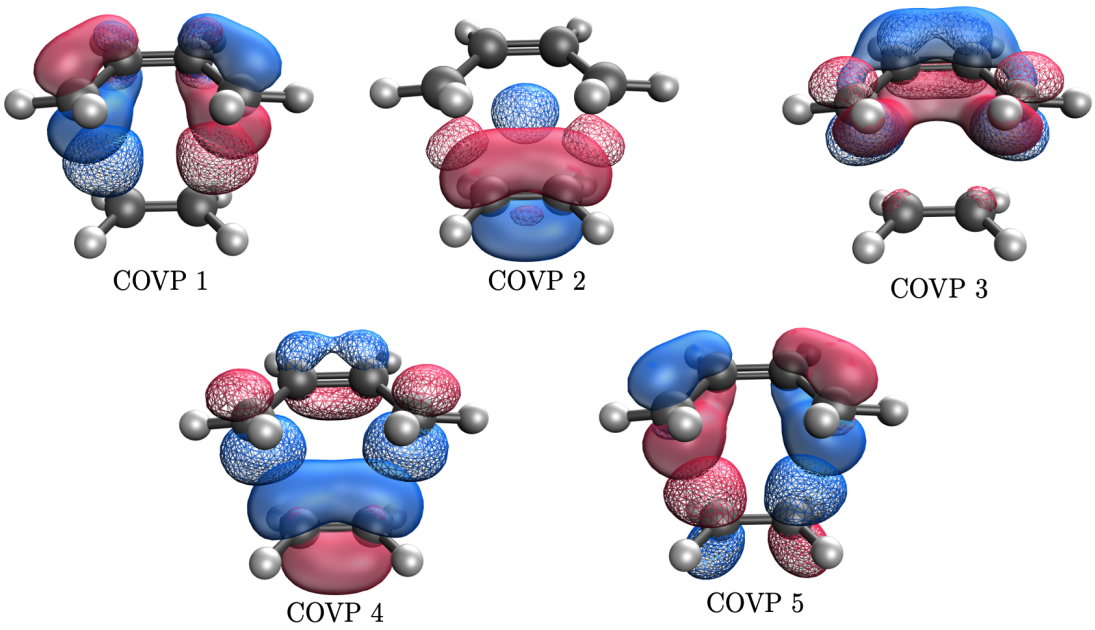

Figure 4: Plots of significant COVPs of 1,3-butadiene and ethene in the POL and CT processes. COVPs 1-3 describe polarization, while COVPs 4,5 describe CT. The occupied orbital of each pair is shown as a solid surface, while the virtual orbital is meshed.

Examining the significant COVPs, shown in Fig. 4, can reveal the character of intermolecular interactions. Electrons move from each occupied orbital to the paired virtual orbital. Thus electron density increases in regions where the phases of occupied orbitals and virtual orbitals match, while the electron density decreases in regions where the phases have opposite signs. Based on this interpretation, COVP 1 shows polarization of the HOMO electrons of 1,3-butadiene towards ethene, while COVP 2 shows polarization of HOMO electrons of ethene towards the terminal carbon atoms of 1,3-butadiene. These changes serve as a preparation for bond making. COVP 3 is polarization of butadiene to allow electron accumulation in the C_2-C_3 region of butadiene, which indicates early partial formation of the π bond in the final product cyclohexene. COVPs 4 and 5 demonstrate electron donation from the HOMO of ethene to the LUMO of 1,3-butadiene and from the HOMO of 1,3-butadiene to the LUMO of ethene, respectively, and they indicate the simultaneous formation and breakage of two C−C bonds in the transition structure.

Table 3: Significant NOCV pairs for the POL and CT processes, as well as their associated energy decreases (in kJ/mol) and amounts of transferred charge (in me^-), and the percentage they contribute to the total energy decrease and amount of transferred charge for each process.

Pair	ΔE	$\Delta E/\Delta E_{\mathrm{POL}}(\%)$	ΔQ	$\Delta Q/\Delta Q_{\mathrm{POL}}(\%)$
1	-21.47	69.30	148.16	24.32
2	-14.85	47.93	147.42	24.20
3	8.11	-26.19	95.08	15.61

(a) Significant NOCV pairs for the POL process

Pair	ΔE	$\Delta E/\Delta E_{\mathrm{CT}}(\%)$	ΔQ	$\Delta Q/\Delta Q_{\mathrm{CT}}(\%)$
4	-83.65	48.14	533.80	39.86
5	-80.09	46.09	494.06	36.89

(b) Significant NOCV pairs for the CT process

The significant NOCV pairs also show that the CT process can be compactly described by two pairs alone, while the POL process requires more pairs to describe. Interestingly, one significant NOCV pair for the POL process actually increases the energy. This suggests that the POL process is fundamentally a collective electron response, where different flows of electrons are balanced to decrease the system energy to the maximal extent possible.

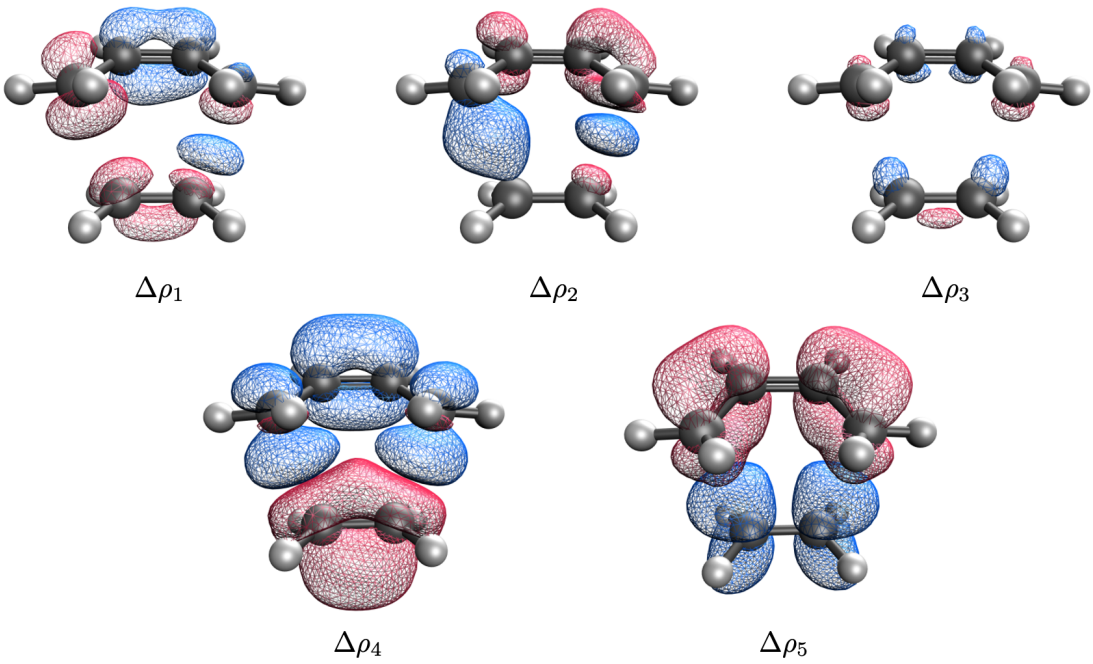

Figure 5: Plots of NOCV density differences of significant NOCV pairs of 1,3-butadiene and ethene in the POL and CT process. $\Delta\rho_1 - \Delta\rho_3$ describe polarization, while $\Delta\rho_4 - \Delta\rho_5$ describe CT. Increases in density are shown in blue while decreases are shown in red.

The significant NOCV pairs for the POL process are complicated and hard to interpret. It is more meaningful to look at their associated density differences, shown in Fig. 5 which altogether describes the polarization of electrons on the terminal carbons of 1,3-butadiene and ethene as well as the accumulation of electrons in the $C_2{-}C_3$ region of 1,3-butadiene. Therefore, the NOCVs tell the same story as the COVPs, but in a more mixed way. In the CT process, the NOCVs with positive eigenvalues can be regarded as bonding orbitals, while those with negative eigenvalues as anti-bonding orbitals. The density difference plots clearly show electron flow from the HOMO of ethene to the LUMO of 1,3-butadiene and from the HOMO of 1,3-butadiene to the LUMO of ethene. Therefore, the NOCV plots and NOCV density difference plots give us the same detailed description as the COVPs about of the inter-molecular interaction of 1,3-butadiene and ethene.

One major advantage of the ALMO-COVP EDA is its ability to perform fragment-wise energy and charge decomposition, since the ALMOs are localized and can be assigned to

different fragments. From Table 4 we can see that polarization is achieved predominantly through electron flows within each fragment, while the charge transfer process is mainly composed of inter-fragment electron flows. These data indicate that the constraints associated with defining the POL state through SCF-MI, and the separate mathematics defining the non-perturbative POL analysis are fundamentally consistent. Butadiene is polarized more than ethene both in terms of energy decrease and amounts of charge rearranged in the POL process, as expected expected since butadiene has delocalized π electrons, which makes it easier to polarize than ethene. The CT process exhibits nearly equal energy and charge transfer between ethene and butadiene, which can be interpreted as a simultaneous partial formation and breakage of two bonds in the transition structure for this Diels-Alder reaction. There are also small electron flows within each fragment during the CT process, which can be regarded as repolarization of each fragment as charge transfer occurs.

Table 4: Fragment-wise energy decrease (in kJ/mol) and the amounts of transferred charge (in me^-), and the percentage they contribute to the total energy decrease and amount of transferred charge for each process.

Donor	Acceptor	ΔE	$\Delta E/\Delta E_{\mathrm{POL}}(\%)$	ΔQ	$\Delta Q/\Delta Q_{\mathrm{POL}}(\%)$
C_4H_6	C_4H_6	-20.29	65.52	20.00	70.32
C_4H_6	C_2H_4	-0.01	0.03	-0.07	-0.25
C_2H_4	C_4H_6	0.19	-0.61	-0.03	-0.11
C_2H_4	C_2H_4	-10.86	35.07	8.53	29.99

(a) Fragment-wise energy and charge decomposition for the POL process.

Donor	Acceptor	ΔE	$\Delta E/\Delta E_{\mathrm{CT}}(\%)$	ΔQ	$\Delta Q/\Delta Q_{\mathrm{CT}}(\%)$
C_4H_6	C_4H_6	-0.48	0.28	-16.66	-6.20
C_4H_6	C_2H_4	-84.58	48.68	143.28	53.28
C_2H_4	C_4H_6	-88.90	51.17	155.69	57.90
C_2H_4	C_2H_4	0.20	-0.12	-13.41	-4.99

(b) Fragment-wise energy and charge decomposition for the CT process.

4.3 The hydrogen bond between water and fluoride ion

The interaction of H_2O molecule with F^- anion is an example of strong hydrogen-bonding, whose strength is more than 6 times greater than the water dimer H-bond. The main EDA results are summarized below in Table 5. Both EDA schemes are able to produce decomposed energies that sum almost exactly to the total energy differences for both the POL and CT processes, confirming the precision of both approaches. However, once again, the amount of rearranged/transferred charge calculated using ALMO-COVP EDA is much smaller than the unrealistically large values obtained from ETS-NOCV EDA.

Table 5: Energies (in kJ/mol) and amounts of transferred charge (in me^-) calculated using ALMO-COVP EDA and ETS-NOCV EDA for the POL and CT processes.

	$E_{\mathrm{POL}} - E_{\mathrm{FRZ}}$	ΔE_{POL}	ΔQ_{POL}	$E_{\mathrm{CT}} - E_{\mathrm{POL}}$	ΔE_{CT}	ΔQ_{CT}
ALMO-COVP EDA	-70.76	-70.76	39.20	-55.18	-55.18	19.75
ETS-NOCV EDA	-70.76	-70.72	625.93	-55.18	-55.18	335.19

The fragment energy and charge decomposition obtained from ALMO-COVP EDA (Table 6) tells us that the polarization energy decrease is due to electron flows within the H_2O molecule and F^- anion, where H_2O is more polarized than F^- (because of the greater perturbation due to charge vs due to dipole). On the other hand, the energy decrease in the CT process is solely due to electron flow from F^- to H_2O. Of course electron flow in hydrogen-bond formation is in the opposite direction of proton donation.

By performing COVP analysis and further breaking the energy decrease and amounts of transferred charge into orbital pairs (Table 7), it is revealed that the POL process is dominated by four significant COVPs while the CT process is compactly described by one COVP. This shows that the POL process is essentially a collective behavior of electrons while the CT process can often be understood in terms of electron flows associated with only a few orbitals.

Table 6: Fragment-wise energy decrease (in kJ/mol) and the amounts of transferred charge (in me^-), and the percentage they contribute to the total energy decrease and amount of transferred charge for each process.

Donor	Acceptor	ΔE	$\Delta E/\Delta E_{\mathrm{POL}}(\%)$	ΔQ	$\Delta Q/\Delta Q_{\mathrm{POL}}(\%)$
H_2O	H_2O	-44.04	62.24	25.84	65.92
H_2O	F^-	0.25	-0.35	-0.29	-0.74
F^-	H_2O	-0.97	1.37	0.14	0.36
F^-	F^-	-26.00	36.74	13.51	34.46

(a) Fragment-wise energy and charge decomposition for the POL process.

Donor	Acceptor	ΔE	$\Delta E/\Delta E_{\mathrm{CT}}(\%)$	ΔQ	$\Delta Q/\Delta Q_{\mathrm{CT}}(\%)$
H_2O	H_2O	-1.76	3.19	0.58	2.94
H_2O	F^-	-0.77	1.40	0.44	2.23
F^-	H_2O	-53.51	96.97	21.32	107.95
F^-	F^-	0.86	-1.56	-2.59	-13.11

(b) Fragment-wise energy and charge decomposition for the CT process.

Table 7: Significant COVPs of the POL and CT processes, as well as their associated energy decrease (in kJ/mol) and amounts of transferred charge (in me^-), and the percentage they contribute to the total energy decrease and amount of transferred charge for each process.

Pair	Donor	Acceptor	ΔE	$\Delta E/\Delta E_{\mathrm{POL}}(\%)$	ΔQ	$\Delta Q/\Delta Q_{\mathrm{POL}}(\%)$
1	H_2O	H_2O	-33.31	47.08	19.50	49.75
2	F^-	F^-	-20.59	29.10	10.53	26.86
3	H_2O	H_2O	-5.32	7.52	3.80	9.70
4	H_2O	H_2O	-4.35	6.15	2.16	5.51

(a) Significant COVPs of POL process

Pair	Donor	Acceptor	ΔE	$\Delta E/\Delta E_{\mathrm{CT}}(\%)$	ΔQ	$\Delta Q/\Delta Q_{\mathrm{CT}}(\%)$
5	F^-	H_2O	-50.94	92.31	20.76	105.12

(b) Significant COVPs of CT process

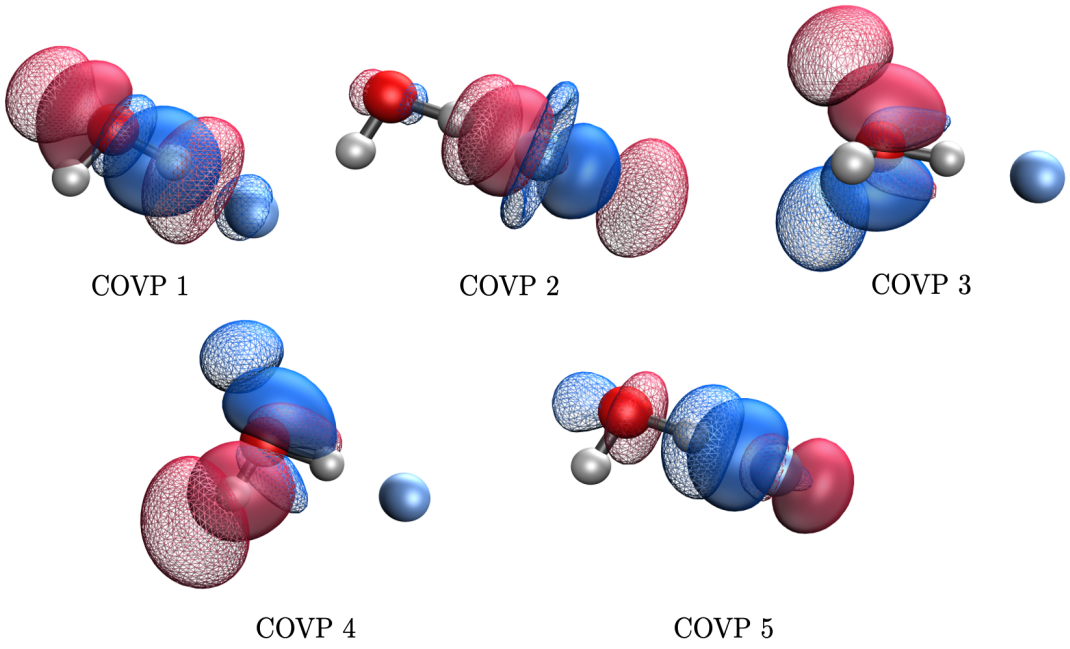

Figure 6: Plots of significant COVPs of H_2O and F^- in the POL process (COVPs 1-4) and the CT process (COVP 5).

The plots of the significant COVPs (Fig. 6) illustrate the nature of these orbitals. COVPs 1,3,4 primarily describe the polarization of H_2O, with COVPs 1 and 4 describe the polarization of occupied levels deriving from sp^2(O) and 1s(H) AOs, while COVP 3 describes the polarization of a 2p(O) orbital. These polarization COVPs displace electrons in H_2O away from F^-, to relieve Pauli repulsions between H_2O and F^-. Consistent with chemical intuition, COVP 1 contributes most to the polarization of H_2O, since electrons in this orbital are closest to the F^- anion. By contrast, COVP 2 describes how the electrons in the 2p orbital of F^- polarize towards the partially positive hydrogen atom of H_2O. COVP 5 describes charge transfer from F^- to H_2O as donation from the 2p orbital of F^- to the adjacent anti-bonding σ(OH) orbital of water. This CT weakens the $O-H$ σ bond and elongates the $O-H$ bond length. Using the same level of theory, the $O-H$ bondlengths of 0.958 Å in isolated water change to 0.957 Å and 1.053 Å in the optimized H_2O-F^- complex, with the longer $O-H$ bond associated with the hydrogen atom adjacent to the F^- anion. The COVP analysis successfully predicted and explained the elongated $O-H$ bond.

Table 8: Significant NOCV pairs of the POL and CT processes, as well as their associated energy decrease (in kJ/mol) and amounts of transferred charge (in me^-), and the percentage they contribute to the total energy decrease and amount of transferred charge for each process.

Pair	ΔE	$\Delta E/\Delta E_{\mathrm{POL}}(\%)$	ΔQ	$\Delta Q/\Delta Q_{\mathrm{POL}}(\%)$
1	-54.13	76.55	215.23	34.39
2	-5.58	7.89	88.53	14.14
3	-4.44	6.28	67.02	10.71

(a) Significant NOCV pairs of POL process

Pair	ΔE	$\Delta E/\Delta E_{\mathrm{CT}}(\%)$	ΔQ	$\Delta Q/\Delta Q_{\mathrm{CT}}(\%)$
4	-50.21	91.00	187.72	51.01

(b) Significant NOCV pairs of CT process

In the NOCV analysis, the POL process is described by 3 significant NOCV pairs while the CT process is again described by 1 significant NOCV pair (Table 8). However, the POL process mostly involves electron flows within a fragment without bond forming and breaking, so it is hard to interpret NOCVs with positive and negative eigenvalues respectively as bonding orbitals and anti-bonding orbitals. Thus NOCV density difference plots (Fig. 7) are more useful to reveal the directions of electron flows during polarization. It is evident that NOCV pair 1 describes the polarization of $2p$ electrons of F^- towards the adjacent H atom, as well as polarization of water valence electron density away from F^-. This picture of the electron flow is similar to COVP 1 and COVP 2 combined, and the energy decrease due to NOCV pair 1 is also very close to the sum of that of COVP 1 and COVP 2. $\Delta\rho_2$ describes the polarization of the oxygen $2p$ orbital away from F^-, which is very similar to COVP 3, both in terms of the direction of electron flows and associated energy decrease. $\Delta\rho_3$ gives a similar picture as COVP 4. $\Delta\rho_4$ describes the density difference of the only significant NOCV pair of the CT process, and it clearly shows an electron transfer from the $2p$ orbital of F^- to the anti-bonding $\sigma^*(\mathrm{O}-\mathrm{H})$ orbital, causing an electron density decrease in the bonding region of the $\mathrm{O}-\mathrm{H}$ bond. This indicates a weakened $\mathrm{O}-\mathrm{H}$ bond due to charge transfer from F^-, as was predicted by the COVP analysis.

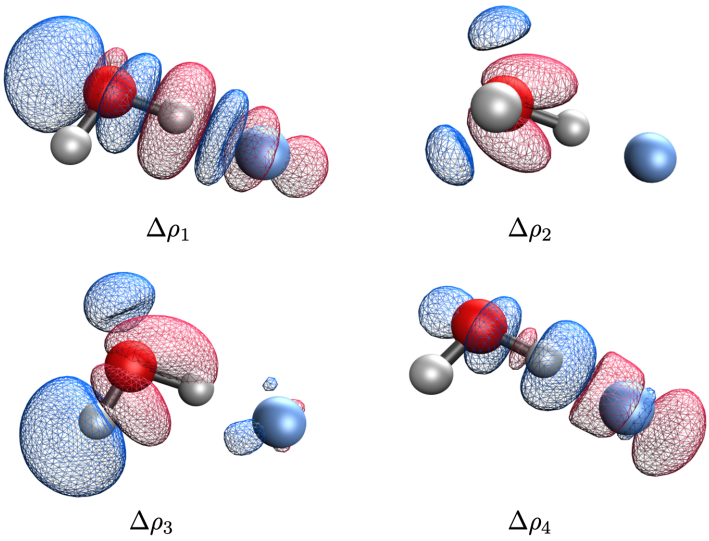

Figure 7: Plots of NOCV density differences of significant NOCV pairs of H_2O and F^- in the POL and CT process. $\Delta\rho_3$ was plotted with isosurface value of ± 0.002 a.u.

4.4 The $H_2O \cdots HF$ Hydrogen Bond

To further explore hydrogen-bonding, we next examine H_2O and HF, with HF being the proton donor and H_2O being the proton acceptor. A summary of the EDA results is presented in Table 9. Again, both EDA schemes give us the numerically exact energy decrease, while the amount of transferred charge is greatly exaggerated by ETS-NOCV EDA. The fragment-wise energy and charge decomposition of ALMO-COVP EDA given in Table 10 tells us that the polarization of H_2O accounts for most of the energy decrease and charge flow in the POL process, while the donation of electrons from H_2O to HF is the dominant source of energy decrease in the CT process.

Table 9: Energies (in kJ/mol) and amounts of transferred charge (in me^-) calculated using ALMO-COVP EDA and ETS-NOCV EDA for the POL and CT process.

	$E_{\mathrm{POL}} - E_{\mathrm{FRZ}}$	ΔE_{POL}	ΔQ_{POL}	$E_{\mathrm{CT}} - E_{\mathrm{POL}}$	ΔE_{CT}	ΔQ_{CT}
ALMO-COVP EDA	-13.46	-13.46	6.35	-18.32	-18.32	5.83
ETS-NOCV EDA	-13.46	-13.46	235.21	-18.32	-18.32	175.04

Table 10: Fragment-wise energy decrease (in kJ/mol) and the amounts of transferred charge (in me^-), and the percentage they contribute to the total energy decrease and amount of transferred charge for each process.

Donor	Acceptor	ΔE	$\Delta E/\Delta E_{\mathrm{POL}}(\%)$	ΔQ	$\Delta Q/\Delta Q_{\mathrm{POL}}(\%)$
H_2O	H_2O	-11.01	81.80	4.86	76.54
H_2O	HF	-0.14	1.04	0.02	0.31
HF	H_2O	-0.00	0.00	-0.02	-0.31
HF	HF	-2.30	17.09	1.48	23.31

(a) Fragment-wise energy and charge decomposition for the POL process.

Donor	Acceptor	ΔE	$\Delta E/\Delta E_{\mathrm{CT}}(\%)$	ΔQ	$\Delta Q/\Delta Q_{\mathrm{CT}}(\%)$
H_2O	H_2O	-0.03	0.16	-2.10	-36.02
H_2O	HF	-17.18	93.78	7.57	129.85
HF	H_2O	-0.91	4.97	0.32	5.49
HF	HF	-0.19	1.04	0.04	0.69

(b) Fragment-wise energy and charge decomposition for the CT process.

Table 11: Significant COVPs of the POL and CT processes, as well as their associated energy decrease (in kJ/mol) and amounts of transferred charge (in me^-), and the percentage they contribute to the total energy decrease and amount of transferred charge for each process.

Pair	Donor	Acceptor	ΔE	$\Delta E/\Delta E_{\mathrm{POL}}(\%)$	ΔQ	$\Delta Q/\Delta Q_{\mathrm{POL}}(\%)$
1	H_2O	H_2O	-8.97	66.64	4.02	63.25
2	HF	HF	-1.60	11.86	1.10	17.39
3	H_2O	H_2O	-1.17	8.69	0.53	8.28

(a) Significant COVPs of POL process

Pair	Donor	Acceptor	ΔE	$\Delta E/\Delta E_{\mathrm{CT}}(\%)$	ΔQ	$\Delta Q/\Delta Q_{\mathrm{CT}}(\%)$
4	H_2O	HF	-16.70	91.16	7.48	128.30

(b) Significant COVPs of CT process

We then performed COVP analysis (summarized in Table 11) to decompose the energy decrease and the amounts of transferred charge and assign them to the most important occupied-virtual pairs of the interaction. Three COVPs make significant contributions to the energy decrease and charge transfer of the POL process, while the CT process can be compactly described by one COVP. This again confirms our interpretation of the POL

process as a collective electronic behavior.

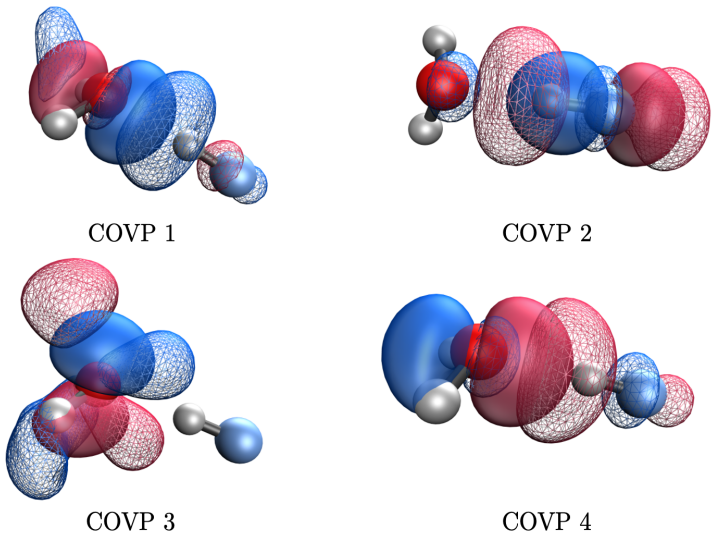

Figure 8: Plots of significant COVPs of H_2O and HF in the POL and CT process.

Referring to Fig. 8, COVPs 1 and 3 describe polarization of O lone pair and valence electrons towards the partially positively charged H atom of HF. By contrast, COVP 2 describes polarization of HF bonding and lone pair electrons away from water to relieve Pauli repulsion with O lone pair electrons. Finally, COVP 4 clearly shows the donation of oxygen lone pair electrons into the anti-bonding $\sigma^*(\mathrm{H}-\mathrm{F})$ orbital, which weakens the $\mathrm{H}-\mathrm{F}$ bond and elongates its bond length. Calculations using the same level of theory results in optimized $\mathrm{H}-\mathrm{F}$ bond lengths of 0.919 Å in isolated HF versus 0.940 Å in $\mathrm{H_2O}\cdots\mathrm{HF}$. COVP analysis again successfully predicts the elongation of the $\mathrm{H}-\mathrm{F}$ bond in hydrogen-bonding, and provides useful insight.

Table 12: Significant NOCV pairs of the POL and CT processes, as well as their associated energy decrease (in kJ/mol) and amounts of transferred charge (in me^-), and the percentage they contribute to the total energy decrease and amount of transferred charge for each process.

Pair	ΔE	$\Delta E/\Delta E_{\mathrm{POL}}(\%)$	ΔQ	$\Delta Q/\Delta Q_{\mathrm{POL}}(\%)$
1	-11.00	81.76	96.51	41.03

(a) Significant NOCV pair of POL process

Pair	ΔE	$\Delta E/\Delta E_{\mathrm{CT}}(\%)$	ΔQ	$\Delta Q/\Delta Q_{\mathrm{CT}}(\%)$
2	-16.69	91.11	103.27	59.00

(b) Significant NOCV pair of CT process

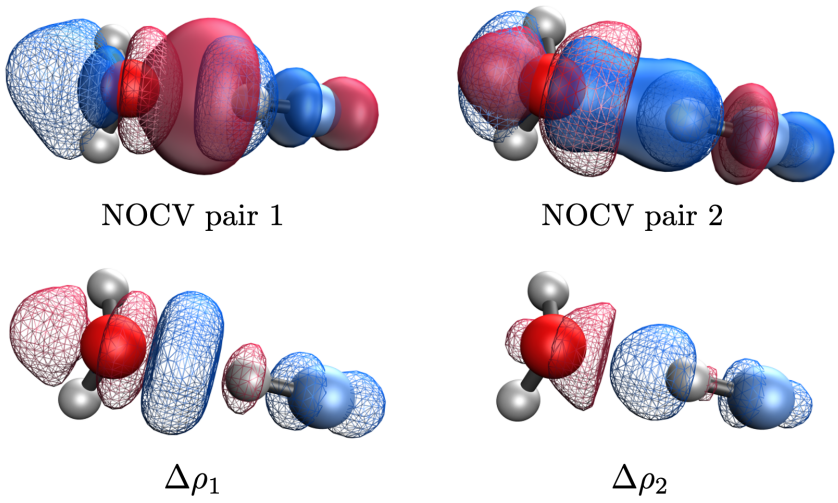

Figure 9: Plots of significant NOCV pairs and associated density differences of H_2O and HF in the POL and CT process.

The significant NOCV pairs (Table 12) of the POL process shows no bonding character, while that of the CT process shows formation of a partial O $\cdots$ H bond. The density difference plot of NOCV pair 1 (Fig. 9) shows polarization of the O lone pair towards HF, as well as polarization of the bonding electrons of HF away from the oxygen atom, to give the same picture as COVPs 1 and 3 combined. $\Delta\rho_2$ shows electron donation from H_2O's oxygen lone pair to the σ^*(HF) orbital during the CT process, causing an electron density decrease in

the $H - F$ bond. This results in the same prediction of a weakened and elongated $H - F$ bond as the COVP analysis.

5 Conclusion

ALMO-COVP EDA and ETS-NOCV EDA are energy decompositions of the DFT energy change between two states of a system (at a given geometry). For an intermolecular complex, there are three states that one can distinguish: a "frozen" state built with the orbitals of isolated monomers, a "polarized" state built with relaxed monomer orbitals that prohibit charge transfer, and an unconstrained (fully relaxed) state. ALMO-COVP EDA and ETS-NOCV EDA use different parameterizations of the energy change. ALMO-COVP EDA uses the generator of the unitary transformation that connects the density matrices of these two states, while ETS-NOCV EDA uses the difference of the two density matrices.

Our analysis reveals several interesting results.

1. We demonstrated that the transition state Fock matrix in ETS-NOCV EDA is an approximation to an effective Fock matrix using only one quadrature point. While the transition state approximation provides accurate energy differences in most cases, it can be systematically improved by using additional quadrature points.

2. We derived exact expressions for the amount of transferred/rearranged charge (in e^-) for both EDA schemes, which mathematically explains why ALMO-COVP EDA provides much smaller amounts of charge transfer than ETS-NOCV EDA. Using a model example ($H_2{}^+$), we demonstrate that the ETS-NOCV values are unphysically large, which is due to the delocalized nature of the NOCVs.

3. Since we generalized the EDA theories to any initial and final state, it is possible to break the relaxation process from the frozen state to the fully relaxed state into several sub-processes by inserting intermediate states. Via a set of examples, we showed that

the polarized state obtained from an SCF-MI calculation is a meaningful intermediate state that correctly separates the polarization and charge transfer processes.

4. We demonstrated that orbital plots of the most important COVPs and the density difference plots of the most important NOCVs are useful tools that provide similar pictures of electron flows in the polarization and charge transfer for several molecular complexes. These include the transition structure for the Diels-Alder cycloaddition of ethene and butadiene, and the hydrogen bonding between water and fluoride anion, and also between water and hydrogen fluoride.

Conflicts of Interest

MH-G is a part-owner of Q-Chem Inc, whose software was used for all developments and calculations reported here.

Acknowledgements

We acknowledge support from the U.S. National Science Foundation through Grant No. CHE-1955643, and additional support from CALSOLV. Hengyuan Shen would thank Yuezhi Mao for helpful discussions.

References

(1) Mardirossian, N.; Head-Gordon, M. Thirty years of density functional theory in computational chemistry: an overview and extensive assessment of 200 density functionals. *Mol. Phys.* **2017**, *115*, 2315–2372.

(2) Neese, F.; Atanasov, M.; Bistoni, G.; Maganas, D.; Ye, S. Chemistry and quantum mechanics in 2019: give us insight and numbers. *J. Am. Chem. Soc.* **2019**, *141*, 2814–2824.

(3) Phipps, M. J.; Fox, T.; Tautermann, C. S.; Skylaris, C.-K. Energy decomposition analysis approaches and their evaluation on prototypical protein–drug interaction patterns. *Chem. Soc. Rev.* **2015**, *44*, 3177–3211.

(4) Pastorczak, E.; Corminboeuf, C. Perspective: Found in translation: Quantum chemical tools for grasping non-covalent interactions. *J. Chem. Phys.* **2017**, *146*, 120901.

(5) Szalewicz, K. Symmetry-adapted perturbation theory of intermolecular forces. *Wiley Interdiscip. Rev.: Comput. Mol. Sci.* **2012**, *2*, 254–272.

(6) Mao, Y.; Loipersberger, M.; Horn, P. R.; Das, A.; Demerdash, O.; Levine, D. S.; Prasad Veccham, S.; Head-Gordon, T.; Head-Gordon, M. From intermolecular interaction energies and observable shifts to component contributions and back again: A tale of variational energy decomposition analysis. *Annu. Rev. Phys. Chem.* **2021**, *72*, 641–666.

(7) Mao, Y.; Horn, P. R.; Head-Gordon, M. Energy decomposition analysis in an adiabatic picture. *Phys. Chem. Chem. Phys.* **2017**, *19*, 5944–5958.

(8) Loipersberger, M.; Mao, Y.; Head-Gordon, M. Variational forward–backward charge transfer analysis based on absolutely localized molecular orbitals: Energetics and molecular properties. *J. Chem. Theory Comput.* **2020**, *16*, 1073–1089.

(9) Morokuma, K. Why do molecules interact? The origin of electron donor-acceptor complexes, hydrogen bonding and proton affinity. *Acc. Chem. Res.* **1977**, *10*, 294–300.

(10) Morokuma, K. Molecular orbital studies of hydrogen bonds. III. C= O··· H–O hydrogen bond in H2CO··· H2O and H2CO··· 2H2O. *J. Chem. Phys.* **1971**, *55*, 1236–1244.

(11) Kitaura, K.; Morokuma, K. A new energy decomposition scheme for molecular interactions within the Hartree-Fock approximation. *Int. J. Quantum Chem.* **1976**, *10*, 325–340.

(12) Ziegler, T.; Rauk, A. On the calculation of bonding energies by the Hartree Fock Slater method. *Theor. Chim. Acta* **1977**, *46*, 1–10.

(13) Ziegler, T.; Rauk, A. A theoretical study of the ethylene-metal bond in complexes between copper (1+), silver (1+), gold (1+), platinum (0) or platinum (2+) and ethylene, based on the Hartree-Fock-Slater transition-state method. *Inorg. Chem.* **1979**, *18*, 1558–1565.

(14) Mitoraj, M. P.; Michalak, A.; Ziegler, T. A combined charge and energy decomposition scheme for bond analysis. *J. Chem. Theory Comput.* **2009**, *5*, 962–975.

(15) Stoll, H.; Wagenblast, G.; Preuβ, H. On the use of local basis sets for localized molecular orbitals. *Theor. Chim. acta* **1980**, *57*, 169–178.

(16) Gianinetti, E.; Raimondi, M.; Tornaghi, E. Modification of the Roothaan equations to exclude BSSE from molecular interaction calculations. *Int. J. Quantum Chem.* **1996**, *60*, 157–166.

(17) Khaliullin, R. Z.; Head-Gordon, M.; Bell, A. T. An efficient self-consistent field method for large systems of weakly interacting components. *J. Chem. Phys.* **2006**, *124*, 204105.

(18) Mo, Y.; Gao, J.; Peyerimhoff, S. D. Energy decomposition analysis of intermolecular interactions using a block-localized wave function approach. *J. Chem. Phys.* **2000**, *112*, 5530–5538.

(19) Mo, Y.; Song, L.; Lin, Y. Block-localized wavefunction (BLW) method at the density functional theory (DFT) level. *J. Phys. Chem. A* **2007**, *111*, 8291–8301.

(20) Mo, Y.; Bao, P.; Gao, J. Energy decomposition analysis based on a block-localized wavefunction and multistate density functional theory. *Phys. Chem. Chem. Phys.* **2011**, *13*, 6760–6775.

(21) Khaliullin, R. Z.; Cobar, E. A.; Lochan, R. C.; Bell, A. T.; Head-Gordon, M. Unravelling the origin of intermolecular interactions using absolutely localized molecular orbitals. *J. Phys. Chem. A* **2007**, *111*, 8753–8765.

(22) Horn, P. R.; Sundstrom, E. J.; Baker, T. A.; Head-Gordon, M. Unrestricted absolutely localized molecular orbitals for energy decomposition analysis: Theory and applications to intermolecular interactions involving radicals. *J. Chem. Phys.* **2013**, *138*, 134119.

(23) Horn, P. R.; Mao, Y.; Head-Gordon, M. Probing non-covalent interactions with a second generation energy decomposition analysis using absolutely localized molecular orbitals. *Phys. Chem. Chem. Phys.* **2016**, *18*, 23067–23079.

(24) Mao, Y.; Levine, D. S.; Loipersberger, M.; Horn, P. R.; Head-Gordon, M. Probing radical–molecule interactions with a second generation energy decomposition analysis of DFT calculations using absolutely localized molecular orbitals. *Phys. Chem. Chem. Phys.* **2020**, *22*, 12867–12885.

(25) Horn, P. R.; Head-Gordon, M. Polarization contributions to intermolecular interactions revisited with fragment electric-field response functions. *J. Chem. Phys.* **2015**, *143*, 114111.

(26) Mitoraj, M.; Michalak, A. Natural orbitals for chemical valence as descriptors of chemical bonding in transition metal complexes. *J. Mol. Model.* **2007**, *13*, 347–355.

(27) Nalewajski, R. F. Internal and external eigenvalue problems of Hermitian operators and their use in electronic structure theory. *Journal of mathematical chemistry* **2008**, *44*, 802–815.

(28) Nalewajski, R. F. *Perspectives in electronic structure theory*; Springer Science & Business Media, 2012.

(29) Khaliullin, R. Z.; Bell, A. T.; Head-Gordon, M. Analysis of charge transfer effects in molecular complexes based on absolutely localized molecular orbitals. *J. Chem. Phys.* **2008**, *128*, 184112.

(30) Veccham, S. P.; Lee, J.; Mao, Y.; Horn, P. R.; Head-Gordon, M. A non-perturbative pairwise-additive analysis of charge transfer contributions to intermolecular interaction energies. *Phys. Chem. Chem. Phys.* **2021**, *23*, 928–943.

(31) Mitoraj, M. P.; Parafiniuk, M.; Srebro, M.; Handzlik, M.; Buczek, A.; Michalak, A. Applications of the ETS-NOCV method in descriptions of chemical reactions. *J. Mol. Model.* **2011**, *17*, 2337–2352.

(32) De Silva, P.; Korchowiec, J. Energy partitioning scheme based on self-consistent method for subsystems: Populational space approach. *J. Comput. Chem.* **2011**, *32*, 1054–1064.

(33) Azar, R. J.; Horn, P. R.; Sundstrom, E. J.; Head-Gordon, M. Useful lower limits to polarization contributions to intermolecular interactions using a minimal basis of localized orthogonal orbitals: Theory and analysis of the water dimer. *J. Chem. Phys.* **2013**, *138*, 084102.

(34) Lao, K. U.; Herbert, J. M. Energy decomposition analysis with a stable charge-transfer term for interpreting intermolecular interactions. *J. Chem. Theory Comput.* **2016**, *12*, 2569–2582.

(35) Mao, Y.; Ge, Q.; Horn, P. R.; Head-Gordon, M. On the computational characterization of charge-transfer effects in noncovalently bound molecular complexes. *J. Chem. Theory Comput.* **2018**, *14*, 2401–2417.

(36) Stone, A. J. Natural bond orbitals and the nature of the hydrogen bond. *J. Phys. Chem. A* **2017**, *121*, 1531–1534.

(37) Ronca, E.; Belpassi, L.; Tarantelli, F. A quantitative view of charge transfer in the hydrogen bond: the water dimer case. *ChemPhysChem* **2014**, *15*, 2682–2687.

(38) Head-Gordon, M.; Maslen, P. E.; White, C. A. A tensor formulation of many-electron theory in a nonorthogonal single-particle basis. *J. Chem. Phys.* **1998**, *108*, 616–625.

(39) Radoń, M. On the properties of natural orbitals for chemical valence. *Theor. Chem. Acc.* **2008**, *120*, 337–339.

(40) Hutter, J.; Parrinello, M.; Vogel, S. Exponential transformation of molecular orbitals. *J. Chem. Phys.* **1994**, *101*, 3862–3865.

(41) Van Voorhis, T.; Head-Gordon, M. A geometric approach to direct minimization. *Mol. Phys.* **2002**, *100*, 1713–1721.

(42) Epifanovsky, E.; Gilbert, A. T.; Feng, X.; Lee, J.; Mao, Y.; Mardirossian, N.; Pokhilko, P.; White, A. F.; Coons, M. P.; Dempwolff, A. L., et al. Software for the frontiers of quantum chemistry: An overview of developments in the Q-Chem 5 package. *J. Chem. Phys.* **2021**, *155*, 084801.

(43) Chai, J.-D.; Head-Gordon, M. Long-range corrected hybrid density functionals with damped atom–atom dispersion corrections. *Phys. Chem. Chem. Phys.* **2008**, *10*, 6615–6620.

(44) Weigend, F.; Ahlrichs, R. Balanced basis sets of split valence, triple zeta valence and quadruple zeta valence quality for H to Rn: Design and assessment of accuracy. *Phys. Chem. Chem. Phys.* **2005**, *7*, 3297–3305.

(45) Rappoport, D.; Furche, F. Property-optimized Gaussian basis sets for molecular response calculations. *J. Chem. Phys.* **2010**, *133*, 134105.

(46) Woon, D. E.; Dunning Jr, T. H. Gaussian basis sets for use in correlated molecular calculations. V. Core-valence basis sets for boron through neon. *J. Chem. Phys.* **1995**, *103*, 4572–4585.

(47) Dunning Jr, T. H. Gaussian basis sets for use in correlated molecular calculations. I. The atoms boron through neon and hydrogen. *J. Chem. Phys.* **1989**, *90*, 1007–1023.

(48) Kendall, R. A.; Dunning Jr, T. H.; Harrison, R. J. Electron affinities of the first-row atoms revisited. Systematic basis sets and wave functions. *J. Chem. Phys.* **1992**, *96*, 6796–6806.

(49) Hunter, J. D. Matplotlib: A 2D graphics environment. *Comput. Sci. Eng.* **2007**, *9*, 90–95.

(50) Behn, A.; Zimmerman, P. M.; Bell, A. T.; Head-Gordon, M. Efficient exploration of reaction paths via a freezing string method. *J. Chem. Phys.* **2011**, *135*, 224108.

(51) Becke, A. D. Density-functional thermochemistry. I. The effect of the exchange-only gradient correction. *J. Chem. Phys.* **1992**, *96*, 2155–2160.

(52) Stephens, P. J.; Devlin, F. J.; Chabalowski, C. F.; Frisch, M. J. Ab initio calculation of vibrational absorption and circular dichroism spectra using density functional force fields. *J. Phys. Chem.* **1994**, *98*, 11623–11627.

(53) Hariharan, P. C.; Pople, J. A. The influence of polarization functions on molecular orbital hydrogenation energies. *Theor. Chim. Acta* **1973**, *28*, 213–222.

(54) Rassolov, V. A.; Pople, J. A.; Ratner, M. A.; Windus, T. L. 6-31G* basis set for atoms K through Zn. *J. Chem. Phys.* **1998**, *109*, 1223–1229.

Table of Contents Graphic